Exponential wave-packet spreading via self-interaction time modulation

Wen-Lei Zhao,[1,2,3,4,5] Jiangbin Gong,[5,*] Wen-Ge Wang,[6,†] Giulio Casati,[7,8] Jie Liu,[2,3,4] and Li-Bin Fu[2,3,4,‡]

[1]*School of Science, Jiangxi University of Science and Technology, Ganzhou 341000, China*

[2]*National Laboratory of Science and Technology on Computational Physics, Institute of Applied Physics and Computational Mathematics, Beijing 100088, China*

[3]*HEDPS, Center for Applied Physics and Technology, Peking University, Beijing 100871, China*

[4]*CICIFSA MoE College of Engineering, Peking University, Beijing 100871, China*

[5]*Department of Physics, National University of Singapore, Singapore 117542*

[6]*Department of Modern Physics, University of Science and Technology of China, Hefei 230026, China*

[7]*Center for Nonlinear and Complex Systems, Università degli Studi dell'Insubria, Via Valleggio 11, 22100 Como, Italy*

[8]*International Institute of Physics, Federal University of Rio Grande do Norte, Natal, Brazil*

The time-periodic modulation of the self-interaction of a Bose–Einstein condensate or a nonlinear optics system has been recognized as an exciting tool to explore interesting physics that was previously unavailable. This tool is exploited here to examine the exotic dynamics of a nonlinear system described by the Gross–Pitaevskii equation. We observe three remarkable and closely related dynamical phenomena, exponentially localized profile of wave functions in momentum space with localization length exponentially increasing in time, exponential wave-packet spreading, and exponential sensitivity to initial conditions. A hybrid quantum-classical theory is developed to partly explain these findings. Time-periodic self-interaction modulation is seen to be a robust method to achieve superfast spreading and induce genuine chaos even in the absence of any external potential.

I. INTRODUCTION

Physics induced by the self-interaction of a Bose–Einstein condensate (BEC) or in nonlinear optics has been a fruitful subject. For example, self-interaction on the mean-field level of a BEC often leads to a subdiffusion of cold-atom wave packets, where the second moment of position (or energy) grows as t^α, with $0 < \alpha < 1$ [1–10]. Even more remarkable, experimental advances in Feshbach resonance [11–14] or waveguide experiments [15,16] have made it possible to actively tune the self-interaction and then explore new phenomena due to time-modulated self-interaction. In particular, time-periodic modulation of the self-interaction of BECs has been recognized as an exciting tool to engineer the Floquet spectrum [17], control many-body tunneling [18], synthesize novel gauge fields [19], etc. Indeed, the so-called many-body coherent destruction of tunneling [18] has been experimentally realized [20] based on fast time-periodic modulation of the self-interaction strength of cold atoms. In nonlinear optics, the spatial modulation of the Kerr nonlinearity (which can be used to simulate time modulation of nonlinearity) was realized by tuning the refractive index of waveguides with the femtosecond laser writing technique [16].

Here we exploit time-periodic modulation of the self-interaction of an optics system or a BEC on the mean-field level to expose three related dynamical phenomena. The results are of general interest to both theoretical studies and cold-atom-based as well as nonlinear optics experiments. In particular, (i) analogous to the seminal dynamical localization physics [21] in cold-atom realizations of kicked-rotor systems

[22], the main localization profile of the time-evolving wave functions in momentum space is found to be exponential; (ii) exponential wave-packet spreading is found to be typical, and its coexistence with exponential wave-function profile is explained in terms of an exponential increase of the localization length in time; (iii) the time evolution is found to be genuinely chaotic because it displays true exponential sensitivity to initial conditions, with the computationally found (finite-time) Lyapunov exponent the same as the rate characterizing the wave-packet spreading for the same timescale. We further use a hybrid quantum-classical theory to shed light on our findings. Our detailed results and theoretical analysis advanced, both quantitatively and qualitatively, a previous work [23] also studying periodic self-interaction modulation.

The exponential wave-packet spreading may offer an alternative route towards superfast heating of particles [24]. Heating up atoms rapidly can suppress the loss of particles from a trap during the heating process. A system of particles after superfast heating, once placed in contact with a cooler system, can be useful for studies of nonequilibrium statistical mechanics. Because the exponential wave-packet spreading is achieved by sole self-interaction modulation in time, it does not need the type of the near-resonance condition advocated in Ref. [25]) and is hence a more robust method than before. Finally, although the dynamics of a system described by the Gross–Pitaevskii equation should be able to exhibit true chaos considering its nonlinear time evolution, this work gives a fascinating example displaying exponential sensitivity without an external potential.

II. MODEL AND RESULTS

Consider a propagating wave under a periodic boundary condition, with its spatial coordinate given by $-\pi \leqslant \theta \leqslant \pi$. Other than the self-interaction that is periodically modulated,

---

*phygj@nus.edu.sg
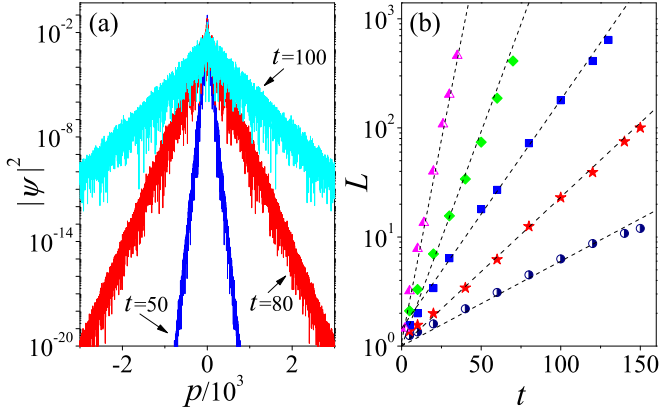†wgwang@ustc.edu.cn
‡lbfu@iapcm.ac.cn

FIG. 1. (a) Exponential profile of the wave functions in momentum space for $g = 1$ and $\hbar_{\text{eff}} = 1$ (on a logarithmic scale), at times $t = 50$ (lower, blue), 80 (middle, red), and 100 (upper, cyan). (b) Exponential increase of the localization length $L(t)$ for $g = 0.6$ (circles), 0.8 (pentagrams), 1.0 (squares), 1.4 (diamonds), and 2.0 (triangles). Dashed lines represent the exponential behavior depicted by Eq. (4).

there is no external potential. The evolution of such a system is assumed to satisfy the following Gross–Pitaevskii equation in dimensionless units,

$$i\hbar_{\text{eff}}\frac{\partial}{\partial t}\psi(\theta,t) = \left[\frac{1}{2}p^2 + g|\psi(\theta,t)|^2 \sum_j \delta(t-j)\right]\psi(\theta,t),$$

(1)

where $p = -i\hbar_{\text{eff}}\frac{\partial}{\partial\theta}$, $\hbar_{\text{eff}}$ is the effective Planck constant, and $g\sum_j \delta(t-j)$ is the periodically modulated self-interaction, with g being the modulation amplitude and $\sum_j \delta(t-j)$ representing delta pulses as a convenient way to modulate the self-interaction.

Let $|\varphi_n\rangle$ be momentum eigenstates, with $p|\varphi_n\rangle = n\hbar_{\text{eff}}|\varphi_n\rangle$, and $\langle\theta|\varphi_n\rangle = e^{in\theta}/\sqrt{2\pi}$. In the representation of $|\varphi_n\rangle$, an arbitrary state can be expressed as $|\psi(\theta,t)\rangle = \sum_{n=-\infty}^{+\infty} \psi_n(t)\langle\theta|\varphi_n\rangle$, with $\psi_n(t)$ being the wave function in the momentum representation. The initial state is taken as a Gaussian wave packet normalized to unity and centered at $\theta = 0$; namely, $\psi(\theta,0) = (a/\pi)^{1/4}\exp(-a\theta^2/2)$. In our numerical simulations, we take $a = 10$. This state decays to virtually zero at $\theta = -\pi$ or $\theta = \pi$ so there is no violation of the periodic boundary condition in θ. Note also that the initial state must be nonuniform in θ in order for the self-interaction to create an effective potential. The one-period evolution operator from $t_{j-1} = j - 1$ to $t_j = j$ is given by

$$U(t_j,t_{j-1}) = e^{-i\frac{H_0}{\hbar_{\text{eff}}}} e^{-i\frac{V(\theta,t_{j-1})}{\hbar_{\text{eff}}}},$$

(2)

where $H_0 = p^2/2$ and $V(\theta,t) = g|\psi(\theta,t)|^2$.

As a typical observation, the wave-function profile in the momentum space after a few modulation periods is found to display an exponential profile over a very broad range of momentum [Fig. 1(a)]. That is, if we take the snapshot of the populations $|\psi_n(t)|^2$ at a particular time t, on average the

populations behave like

$$|\psi_n(t)|^2 \approx \frac{1}{2L(t)}\exp\left[-\frac{|n|}{L(t)}\right],$$

(3)

with some expected fluctuations. On the other hand, Fig. 1(b) indicates that the found localization length $L(t)$ increases exponentially with time, at a rate depending on $\hbar_{\text{eff}}$ and the interaction strength g. Specifically, we find

$$L(t) \approx L_0 e^{\gamma t/2} \text{ with } \gamma \approx \ln[1 + (g/\pi\hbar_{\text{eff}})^2]$$

(4)

if g is not too small (e.g., $g > 0.6$). If g is too small, although the wave-function profile in the momentum space is still exponential, the time dependence of $L(t)$ will not be captured by our following theory based on an assumption of chaos. Equation (4) as the main finding of this work is explained below by a hybrid quantum-classical theory.

III. A HYBRID QUANTUM-CLASSICAL THEORY

Consider first the matrix elements of the self-interaction $V(t)$ in momentum representation:

$$V_{n,m}(t) = g\int d\theta\, \varphi_m^*(\theta)|\psi(\theta,t)|^2\varphi_n(\theta).$$

(5)

A simple calculation yields $V_{n,m}(t) = 2g\,Y_{n-m}(t)$, where $Y_n(t)$ is the wave-function autocorrelation function at time t, with

$$Y_n(t) = \frac{1}{4\pi}\sum_{m=-\infty}^{+\infty}\psi_m^*(t)\psi_{m+n}(t).$$

(6)

This makes it clear that the V matrix in momentum representation has a band structure with a band-width determined by the correlation length of the wave function $\psi_n(t)$. Indeed, as observed in direct numerical calculations, the matrix elements of $V(t)$ outside the band decay to zero rapidly. Such a band structure of $V_{n,m}$ accounts for the exponential profile of $\psi_n(t)$ depicted by Eq. (3). Now a positive feedback mechanism comes into play. It is clear that, if the wave-function profile $\psi_n(t)$ spreads out in momentum space, then its autocorrelation length grows, the bandwidth of the self-interaction V matrix increases accordingly, and as a result the wave packet spreads more at a faster speed.

To turn the above qualitative picture into a quantitative theory, we next make connection between the nonlinear propagator in Eq. (1) and that of a generalized kicked rotor (GKR) model. To that end, note first

$$|\psi(\theta,t)|^2 = 2\sum_{n=-\infty}^{+\infty}Y_n(t)e^{in\theta},$$

(7)

with $Y_n(t)$ defined in Eq. (6). For an initial Gaussian packet which is an even function of θ, the time-evolving state will maintain this symmetry. This gives rise to a real $Y_n(t)$, with $Y_n(t) = Y_{-n}(t)$ [26]. This simplifies the self-interaction potential $V(\theta,t) = g|\psi(\theta,t)|^2$,

$$V(\theta,t) = g|\psi(\theta,t)|^2 = 2gY_0(t) + 4g\sum_{n=1}^{+\infty}Y_n(t)\cos(n\theta).$$

(8)

One can now identify an effective Hamiltonian from Eq. (1) in terms of a GKR; namely,

$$H_{eff} = \frac{p^2}{2} + \sum_{n=1}^{+\infty} K_n(t)\cos(n\theta)\sum_j (t-j), \qquad (9)$$

where $K_n(t) = 4gY_n(t)$, and the term $2gY_0$ also contained in $V(\theta,t)$ is dropped because it is independent of θ and hence only yields trivial overall phases to the time-evolving state at all times. That is, the dynamics of our system is equivalent to that of a GKR, whose kicking potential is given by $\sum_{n=1}^{+\infty} K_n(t)\cos(n\theta)$. This kicking potential is self-adjusting on the fly because it depends on $K_n(t) = 4gY_n(t)$, which changes with the time-evolving state.

To gain further insights, we examine the classical dynamics of the GKR defined in Eq. (9). The associated classical map from t to $t+1$ is given by

$$p_c(t+1) - p_c(t) = \sum_{n=1}^{+\infty} nK_n(t)\sin[n\theta(t)],$$
$$\theta(t+1) - \theta(t) = p_c(t+1), \qquad (10)$$

where p_c stands for classical momentum. For sufficiently large g such that the autocorrelation length of the time-evolving state increases rapidly, the kicking strength $K_n(t)$ of the above classical map quickly increases, resulting in classical chaos. Assuming a random distribution in θ (decorrelated with momentum) due to classical chaos, one immediately has [26]

$$\left\langle p_c^2(t+1)\right\rangle \approx \left\langle p_c^2(t)\right\rangle + \tfrac{1}{2}K_g, \qquad (11)$$

with

$$K_g = \sum_{n=1}^{\infty} [nK_n(t)]^2. \qquad (12)$$

Here $\langle \cdots \rangle$ denotes a classical average over the initial classical Gaussian ensemble. To evaluate K_g, one needs to return to $K_n(t) = 4gY_n(t)$. Assuming the exponential profile of $\psi_n(t)$ depicted in Eq. (3), it can be shown that K_g is proportional to $\frac{g^2}{\pi^2}L^2(t)$, i.e., $K_g = \eta\frac{g^2}{\pi^2}L^2(t)$ with a proportionality prefactor η [26]. This being the case, we arrive at

$$\left\langle p_c^2(t+1)\right\rangle \approx \left\langle p_c^2(t)\right\rangle + \frac{1}{2}\eta\frac{g^2}{\pi^2}L^2(t). \qquad (13)$$

Although the GKR introduced above has a time-dependent kicking strength, there must still be a fair quantum-classical correspondence. Considering the observed exponential increase in $L(t)$ and hence an exponential increase in momentum squared, both classical and quantum dynamics should yield the same exponential rate. Thus, as also confirmed by detailed numerical results after a transient period (see Fig. 2), the quantum momentum squared is expected to be proportional to the mean classical momentum squared,

$$\langle p^2(t)\rangle = \alpha\langle p_c^2(t)\rangle. \qquad (14)$$

The exact values of α as introduced above are not important, and they depend on $\hbar_{eff}$ and g. Applying this to Eq. (13), one
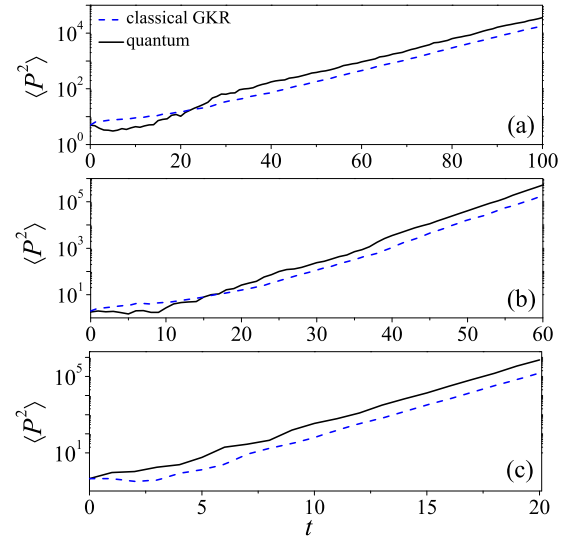

FIG. 2. Comparison in energy between the classical GKR (dashed lines in blue) and the quantum results (solid lines). From top to bottom: $\hbar_{eff} = 1$, 0.6, and 0.3 with $g = 1$. The results indicate that quantum momentum variance is proportional to classical momentum variance after a transient period, both displaying exponential increase.

has

$$\langle p^2(t+1)\rangle \approx \langle p^2(t)\rangle + \frac{1}{2}\alpha\eta\left(\frac{g}{\pi}\right)^2 L^2(t). \qquad (15)$$

As a final step, we use the exponential profile of $\psi_n(t)$ again, which tells us that $\langle p^2(t)\rangle$ is roughly proportional to $\hbar_{eff}^2 L^2(t)$. We thus assume $\langle p^2(t)\rangle = \beta\hbar_{eff}^2 L^2(t)$. Substituting this relation into Eq. (15), an iterative relation emerges as follows:

$$\langle p^2(t+1)\rangle \approx \left[1 + \frac{1}{2}\frac{\alpha\eta}{\beta}\left(\frac{g}{\pi\hbar_{eff}}\right)^2\right]\langle p^2(t)\rangle. \qquad (16)$$

Remarkably, the important ratio $\frac{\alpha\eta}{\beta}$ above tends to approach a rather universal value if $L(t)$ increases exponentially, i.e., $\frac{\alpha\eta}{\beta} \approx 2$ after a transient period [26], regardless of other system parameters. Equation (16) then yields our main theoretical result, i.e.,

$$\langle p^2(t)\rangle \sim e^{\gamma t}, \qquad (17)$$

where

$$\gamma \approx \ln[1 + (g/\pi\hbar_{eff})^2]. \qquad (18)$$

This also accounts for the time dependence of $L(t)$ observed earlier [see Eq. (4)], as supported by a comparison between numerics and theory in Fig. 1(b). That is, the momentum squared increases exponentially with an exponent γ, which explains quantitatively why the localization length $L(t)$ increases exponentially with an exponent $\gamma/2$. This derived exponent based on a hybrid quantum-classical theory depends on the self-interaction strength g and $\hbar_{eff}$. Preparing the system in different regimes with different $\hbar_{eff}$ will result in different exponential behavior.
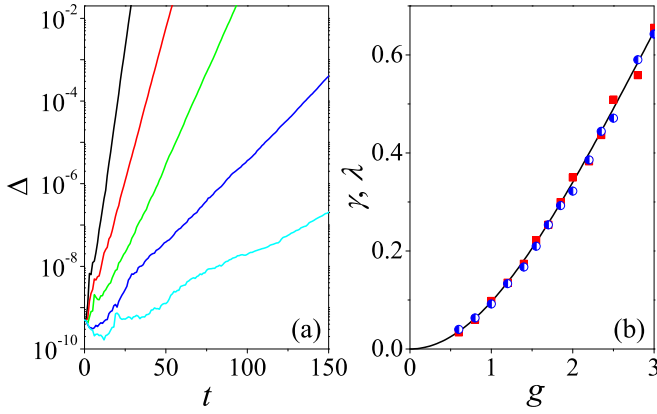
FIG. 3. (a) The distance $\Delta(t)$ between two wave packets versus time (on a logarithmic scale), starting from two very close initial conditions, $\hbar_{\text{eff}} = 1$. From top to bottom: $g = 3$ (black), 2 (red), 1.5 (green), 1 (blue), and 0.7 (cyan). (b) The extracted exponential rate γ (solid squares) versus the coupling strength g as compared with the theoretical value (solid curve) given in Eq. (18). Numerical values of γ are extracted from $L(t)$ as plotted in Fig. 1(b). The circles denote the Lyapunov exponent λ calculated from Eq. (19). All of them are in excellent agreement.

IV. GENUINE "QUANTUM" CHAOS

In linear systems and at least on the wave-function level, there is no exponential sensitivity to initial states. However, the Gross–Pitaevskii equation here is nonlinear and exponential sensitivity to initial conditions might occur. It is then curious to check whether the exponential wave-packet spreading can be quantitatively connected with Lyapunov instability of our system. In particular, we define the (finite-time) Lyapunov exponent as

$$\lambda = -\lim_{t \to t_f} \lim_{\Delta_0 \to 0} \frac{1}{t_f} \ln \frac{\Delta(t_f)}{\Delta_0}, \quad (19)$$

where t_f is the total time during which one may numerically track the time evolution, $\Delta(t) = 1 - |\langle \psi_1(\theta,t)|\psi_2(\theta,t)\rangle|^2$ is a natural measure of the distance between two time-evolving states $\psi_1(\theta,t)\psi_2(\theta,t)$, with $\psi_1(\theta,t)$ and $\psi_2(\theta,t)$ emanating from two slightly different initial conditions. We note that in our numerical experiments t_f is on the scale of hundreds of kicking periods due to the rather fast wave-packet exponential spreading.

Figure 3(a) shows that Δ also increases exponentially with time. The obtained (finite-time) Lyapunov exponents are plotted in Figure 3(b) as a function of g. It is seen that the numerically obtained Lyapunov exponents λ agree perfectly with the γ exponent derived earlier [see Eq. (18)]. This further justifies our early hybrid quantum-classical treatment. On the one hand, it is now seen that, in a system with periodic self-interaction modulation, genuine exponential sensitivity might occur in the absence of any external potential. On the other hand, exponential increase of the localization length $L(t)$, exponential wave-packet spreading, and the exponential sensitivity to initial conditions can now all be connected with the same exponent γ.

V. SUMMARY

In a simple dynamical model relevant to nonlinear optics and mean-field descriptions of BEC, we have shown that exponential wave-packet spreading can coexist with (mainly) exponential wave-function profiles in the momentum space, with the localizing length exponentially increasing in time. The found exponent characterizing the exponential behavior can be derived via a hybrid quantum-classical theory. The found exponent is the same as the positive (finite-time) Lyapunov exponent characterizing the exponential sensitivity to initial conditions in the absence of any external potential.

APPENDIX A: ON THE CORRELATION FUNCTION Y_n

In this appendix, we show detailed derivations of some properties of wave-packet spreading studied in the main text. In Appendix A, we discuss properties of the correlation function $Y_n(t)$ defined in the main text. In Appendix B, we present some detailed theoretical derivations together with their justifications.

We start with the wave-function expansion $\psi(\theta,t) = \sum_{n=-\infty}^{+\infty} \psi_n(t)e^{in\theta}/\sqrt{2\pi}$, which gives

$$|\psi(\theta,t)|^2 = 2 \sum_{n=-\infty}^{+\infty} Y_n(t)e^{in\theta}, \quad (A1)$$

where

$$Y_n(t) = \frac{1}{4\pi} \sum_{m=-\infty}^{+\infty} \psi_m^*(t)\psi_{m+n}(t) \quad (A2)$$

is the correlation function discussed in the main text. Equation (A1) shows that $Y_n(t)$ is basically a Fourier transform of $|\psi(\theta,t)|^2$, i.e., $Y_n(t) = \frac{1}{\sqrt{8\pi}} \int_0^{2\pi} d\theta \frac{1}{\sqrt{2\pi}} |\psi(\theta,t)|^2 e^{-in\theta}$. The initial state we consider is a Gaussian wave packet, which is symmetric with respect to reflection, i.e., $\psi(-\theta,0) = \psi(\theta,0)$. Because the time evolution respects this symmetry at all times t, one has $\psi_n(t) = \psi_{-n}(t)$ and

$$Y_n(t) = Y_{-n}(t). \quad (A3)$$

Moreover, $Y_n(t)$ is real, since $Y_n^*(t) = \frac{1}{\sqrt{8\pi}} \int_0^{2\pi} d\theta \frac{1}{\sqrt{2\pi}} |\psi(\theta,t)|^2 e^{in\theta} = Y_{-n}(t) = Y_n(t)$. From Eq. (A2), the correlation function Y_n can be written as

$$Y_n(t) = \frac{1}{4\pi} \left[\sum_{m=0}^{+\infty} \psi_m^*(t)\psi_{m+n}(t) + \sum_{m=-\infty}^{-n} \psi_m^*(t)\psi_{m+n}(t) + \sum_{m=-(n-1)}^{-1} \psi_m^*(t)\psi_{m+n}(t) \right]. \tag{A4}$$

The second term in the above equation can be rewritten as

$$\sum_{m=-\infty}^{-n} \psi_m^*(t)\psi_{m+n}(t) = \sum_{m=0}^{+\infty} \psi_{-(m+n)}^*(t)\psi_{-m}(t). \tag{A5}$$

The last term in Eq. (A4) takes the form

$$\sum_{m=-(n-1)}^{-1} \psi_m^*(t)\psi_{m+n}(t) = \sum_{m=1}^{n-1} \psi_{-m}^*(t)\psi_{-m+n}(t)$$

$$= \begin{cases} \sum_{m=1}^{k-1} [\psi_{-m}^*(t)\psi_{-m+n}(t) + \psi_{-n+m}^*(t)\psi_m(t)] + |\psi_k(t)|^2 & \text{for } n = 2k, \quad k = 1,2,\ldots \\ \sum_{m=1}^{k} [\psi_{-m}^*(t)\psi_{-m+n}(t) + \psi_{-n+m}^*(t)\psi_m(t)] & \text{for } n = 2k+1, \quad k = 0,1,2,\ldots. \end{cases} \tag{A6}$$

Then, we have the following expression for Y_n,

$$Y_n = \frac{1}{4\pi} \begin{cases} \sum_{m=0}^{+\infty} [\psi_m^*(t)\psi_{m+n}(t) + \psi_{-(m+n)}^*(t)\psi_{-m}(t)] \\ \quad + \sum_{m=1}^{k-1} [\psi_{-m}^*(t)\psi_{-m+n}(t) + \psi_{-n+m}^*(t)\psi_m(t)] + |\psi_k(t)|^2 & \text{for } n = 2k, \quad k = 1,2,\ldots \\ \sum_{m=0}^{+\infty} [\psi_m^*(t)\psi_{m+n}(t) + \psi_{-(m+n)}^*(t)\psi_{-m}(t)] \\ \quad + \sum_{m=1}^{k} [\psi_{-m}^*(t)\psi_{-m+n}(t) + \psi_{-n+m}^*(t)\psi_m(t)] & \text{for } n = 2k+1, \quad k = 0,1,2,\ldots. \end{cases} \tag{A7}$$

By using the symmetry $\psi_n(t) = \psi_{-n}(t)$, one finds that $\psi_{-(m+n)}^*(t)\psi_{-m}(t) = \psi_{m+n}^*(t)\psi_m(t)$ and that $\psi_{-m}^*(t)\psi_{-m+n}(t) = \psi_m^*(t)\psi_{m-n}(t)$. Then, from Eq. (A7) one has

$$Y_n(t) = \frac{1}{4\pi} \begin{cases} \sum_{m=0}^{+\infty} [\psi_m^*(t)\psi_{n+m}(t) + \text{c.c.}] \\ \quad + \sum_{m=1}^{k-1} [\psi_m(t)\psi_{-n+m}^*(t) + \text{c.c.}] \\ \quad + |\psi_k(t)|^2 & \text{for } n = 2k, \quad k = 1,2,\ldots \\ \sum_{m=0}^{+\infty} [\psi_m^*(t)\psi_{n+m}(t) + \text{c.c.}] \\ \quad + \sum_{m=1}^{k} [\psi_m(t)\psi_{-n+m}^*(t) + \text{c.c.}] & \text{for } n = 2k+1, \quad k = 0,1,2,\ldots, \end{cases} \tag{A8}$$

where c.c. denotes complex conjugation and $Y_0 = \frac{1}{4\pi}$. Rewriting $Y_n(t)$ in the above form helps us to make approximations later on.

Noting next the exponential profile $|\psi_n(t)|^2$ shown in the main text. Neglecting any subtle structure in the wave-function profile, the wave function can be approximately written as

$$\psi_n(t) \approx a\sqrt{\frac{1}{2L(t)}} \exp\left(-\frac{|n|}{2L(t)}\right) \exp(-i\phi_n), \tag{A9}$$

where ϕ_n are the phases. Here, we introduce the parameter a to account for fluctuations of the wave function around the exponential profile. Numerically, for large-momentum components, these fluctuations tend to be uniform in n and also in time for the time duration studied here. Therefore, we can approximately take a as a uniformly distributed random number. We have also checked that the phases ϕ_n can be effectively regarded as random numbers as well.

Due to the relation $Y_n = Y_{-n}$, it is sufficient to discuss Y_n for $n > 0$ only. Making use of the expression in Eq. (A9), we arrive at

$$\psi_m^*(t)\psi_{n+m}(t) + \text{c.c.} \approx \frac{a^2}{L(t)} \exp\left[-\frac{m}{L(t)}\right] \exp\left[-\frac{n}{2L(t)}\right] \cos(\phi_m - \phi_{n+m}) \text{ for } m > 0, \tag{A10}$$

and

$$\psi_m(t)\psi_{-n+m}^*(t) + \text{c.c.} \approx \frac{a^2}{L(t)} \exp\left[-\frac{n}{2L(t)}\right] \cos(\phi_m - \phi_{m-n}) \text{ for } n > m > 0. \tag{A11}$$

Substitution of Eqs. (A10) and (A11) into Eq. (A8) yields

$$Y_n(t) \approx \frac{a^2}{8\pi L(t)} \exp\left[-\frac{n}{2L(t)}\right] F(n), \tag{A12}$$

where

$$F(n) = \begin{cases} 1 + 2\left[\sum_{m=0}^{+\infty} e^{-\frac{m}{L(t)}} \cos(\phi_m - \phi_{n+m}) + \sum_{m=1}^{k-1} \cos(\phi_m - \phi_{n-m}) \right] & \text{for } n = 2k, \quad k = 1, 2, \ldots \\ 2\left[\sum_{m=0}^{+\infty} e^{-\frac{m}{L(t)}} \cos(\phi_m - \phi_{n+m}) + \sum_{m=1}^{k} \cos(\phi_m - \phi_{n-m}) \right] & \text{for } n = 2k + 1, \quad k = 0, 1, 2, \ldots. \end{cases} \tag{A13}$$

We have checked this prediction numerically [see Fig. 4(a) here]. Equation (A12) will be used in the next section in the study of the GKR model. In particular, the factor one in the above $F(n)$ expression in the case of even n will be neglected.

APPENDIX B: DERIVATION OF γ

The Hamiltonian of the GKR model described the main text reads

$$H_{\text{eff}} = \frac{p^2}{2} + \left[\sum_{n=1}^{+\infty} K_n(t) \cos(n\theta) \right] \sum_j (t - j), \tag{B1}$$

where $K_n(t) = 4g Y_n(t)$. This leads to the following classical mapping:

$$p_c(t+1) - p_c(t) = \sum_{n=1}^{+\infty} n K_n(t) \sin[n\theta(t)],$$
$$\theta(t+1) - \theta(t) = p_c(t+1), \tag{B2}$$

where $p_c(t)$ and $\theta(t)$ represent the (angular) momentum and the angle after the tth kick, respectively. Note that, in the following derivation, for brevity, we use K_n^t to replace $K_n(t)$, and θ_t to $\theta(t)$. From Eq. (B2), one obtains

$$p_c(t+1) = p_c(t) + \sum_{n=1}^{+\infty} n K_n^t \sin(n\theta_t)$$
$$= p_c(0) + \sum_{i=0}^{t} \sum_{n=1}^{+\infty} n K_n^i \sin(n\theta_i). \tag{B3}$$
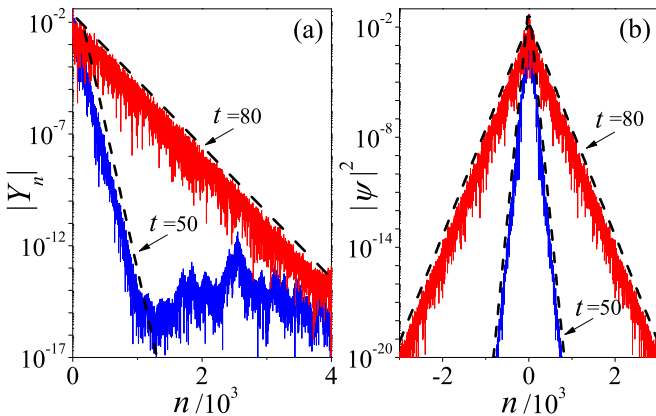

FIG. 4. (a) The correlation function $|Y_n|$ for $\hbar_{\text{eff}} = 1$, $g = 1$ at $t = 50$ (blue) and 80 (red). Dashed lines indicate exponential decay $\exp(-\frac{n}{2L})$. (b) The corresponding momentum distributions. Dashed lines (in black) indicate exponential decay $\exp(-\frac{n}{L})$.

Then, the momentum variance is found to be

$$\langle p_c^2(t+1) \rangle = \left\langle \left[p_c(0) + \sum_{i=0}^{t} \sum_{n=1}^{+\infty} n K_n^i \sin(n\theta_i) \right]^2 \right\rangle$$
$$= \langle p_c^2(0) \rangle + 2 p_c(0) \sum_{i=0}^{t} \sum_{n=1}^{+\infty} n K_n^i \langle \sin(n\theta_i) \rangle$$
$$+ \left\langle \sum_{i=0}^{t} \left[\sum_{n=1}^{+\infty} n K_n^i \sin(n\theta_i) \right]^2 \right\rangle$$
$$+ \left\langle \sum_{\substack{\mu,\nu=0 \\ \mu \neq \nu}}^{t} \left[\sum_{n=1}^{+\infty} n K_n^\mu \sin(n\theta_\mu) \right] \right.$$
$$\left. \times \left[\sum_{n=1}^{+\infty} n K_n^\nu \sin(n\theta_\nu) \right] \right\rangle, \tag{B4}$$

where $\langle \cdots \rangle$ means ensemble average over classical trajectories. One should note that, in the last line of the above equation, since $\mu \neq \nu$, the two summations in the two brackets [·] correspond to different times. When the classical system undergoes a chaotic motion, this term decays exponentially with time. According to the random-phase approximation, $\langle \sin(n\theta_i) \rangle = 0$. Then, the momentum variance can be approximately written as

$$\langle p_c^2(t+1) \rangle \approx \langle p_c^2(0) \rangle + \left\langle \sum_{i=0}^{t} \left[\sum_{n=1}^{+\infty} n K_n^i \sin(n\theta_i) \right]^2 \right\rangle$$
$$= \langle p_c^2(0) \rangle + \sum_{i=0}^{t} \sum_{n=1}^{+\infty} n^2 (K_n^i)^2 \langle \sin^2(n\theta_i) \rangle$$
$$+ \sum_{i=0}^{t} \sum_{\substack{m,n=1 \\ m \neq n}}^{+\infty} mn K_m^i K_n^i \langle \sin(m\theta_i) \sin(n\theta_i) \rangle. \tag{B5}$$

Since

$$\langle \sin^2(n\theta_i) \rangle = \frac{1}{2\pi} \int_0^{2\pi} \sin^2(n\theta_i) d\theta_i = \frac{1}{2}, \tag{B6}$$

$$\langle \sin(m\theta_i) \sin(n\theta_i) \rangle = \frac{1}{2} \langle \cos[(m-n)\theta_i]$$
$$- \cos[(m+n)\theta_i] \rangle \overset{m \neq n}{=} 0, \tag{B7}$$

we get from Eq. (B5),

$$\langle p_c^2(t+1) \rangle \approx \langle p_c^2(0) \rangle + \frac{1}{2} \sum_{i=0}^{t} \sum_{n=1}^{+\infty} n^2 (K_n^i)^2. \tag{B8}$$
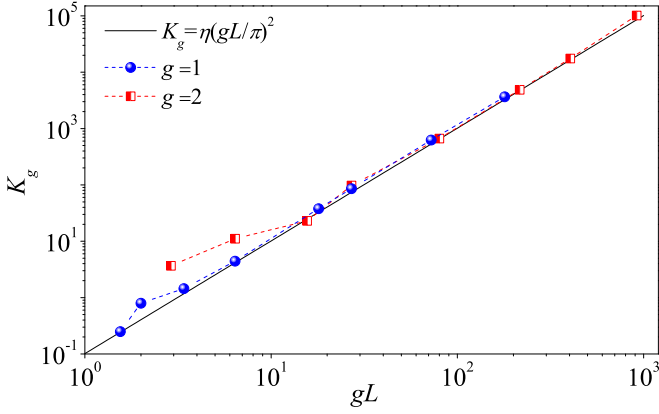
FIG. 5. Linear dependence of K_g on $(gL)^2$ with $\hbar_{\text{eff}} = 1$. The solid straight line denotes $K_g = \eta(gL/\pi)^2$ with $\eta \approx 1$.

That is,

$$\langle p_c^2(t+1)\rangle \approx \langle p_c^2(t)\rangle + \tfrac{1}{2}K_g, \qquad \text{(B9)}$$

where

$$K_g = \sum_{n=1}^{\infty} \left(n K_n^t\right)^2. \qquad \text{(B10)}$$

Next we discuss the relation between K_g and $L^2(t)$. Note that $K_n^t = 4gY_n(t)$ and $Y_n(t)$ is already derived in Eq. (A12). Then, for sufficiently large $L(t)$, we drop the first factor of one in the $F(n)$ expression for $n = 2k$ [see Eq. (A13)], obtaining an approximate K_g

$$
K_g \approx \frac{g^2}{\pi^2 L^2(t)} \sum_{n=1}^{+\infty} a^4 n^2 \exp\left[-\frac{n}{L(t)}\right]
$$
$$
\times \left[\sum_{m=0}^{+\infty} e^{-\frac{m}{L(t)}} \cos\left(\phi_m - \phi_{n+m}\right)\right.
$$
$$
\left. + \sum_{m=1}^{k} \cos\left(\phi_m - \phi_{n-m}\right)\right]^2, \qquad \text{(B11)}
$$

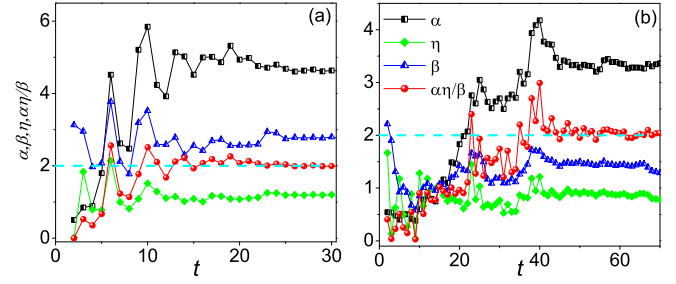FIG. 6. Coefficients α, β, η and $\alpha\eta/\beta$ versus time for (a) $\hbar_{\text{eff}} = 0.3$ and (b) 0.6 with $g = 1$. The dashed straight line (in cyan) denotes that $\alpha\eta/\beta = 2$.

where $k = n/2$ for even n and $k = (n-1)/2$ for odd n. The effective randomness of ϕ_m implies that

$$\sum_{m=0}^{+\infty} e^{-\frac{m}{L(t)}} \cos\left(\phi_m - \phi_{n+m}\right) \sim \sqrt{L(t)}, \qquad \text{(B12)}$$

and

$$\sum_{m=1}^{k} \cos\left(\phi_m - \phi_{n-m}\right) \sim \sqrt{k} \sim \sqrt{n}. \qquad \text{(B13)}$$

Due to the rapid decay of $e^{-n/L(t)}$, the main contribution to the summation over n in Eq. (B11) comes from the region $[1, \varepsilon L]$, where ε is of the order of 1. Plugging the estimates of Eq. (B12) and Eq. (B13) into Eq. (B11) and performing the summation over n, one arrives at the following estimate:

$$K_g = \eta\left(\frac{g}{\pi}\right)^2 L^2(t), \qquad \text{(B14)}$$

where η is a proportionality constant (which is used in the main text). Numerically, as shown in Fig. 5, we have verified that K_g indeed has a linear dependence on $(gL)^2$.

In the main text, there are three prefactors η, α, and β introduced to help us to develop a hybrid quantum-classical theory. Their detailed time dependence in two typical examples are shown in Fig. 6 of this appendix. There it is seen that, after a transient period, $\alpha\eta/\beta$ approaches a rather universal value that is approximately two, for different values of $\hbar_{\text{eff}}$ and g (that give different individual values of α, η, and β). It is this empirical observation $\alpha\eta/\beta \approx 2$ that further simplifies our hybrid quantum-classical theory in the main text, with the theoretical result of the exponential rate in agreement numerical experiments.

[1] M. I. Molina, Phys. Rev. B **58**, 12547 (1998).

[2] D. L. Shepelyansky, Phys. Rev. Lett. **70**, 1787 (1993); I. García-Mata and D. L. Shepelyansky, Phys. Rev. E **79**, 026205 (2009).

[3] A. S. Pikovsky and D. L. Shepelyansky, Phys. Rev. Lett. **100**, 094101 (2008).

[4] M. Mulansky and A. Pikovsky, Europhys. Lett. **84**, 10006 (2008).

[5] S. Flach, D. O. Krimer, and Ch. Skokos, Phys. Rev. Lett. **102**, 024101 (2009).

[6] J. D. Bodyfelt, T. V. Laptyeva, Ch. Skokos, D. O. Krimer, and S. Flach, Phys. Rev. E **84**, 016205 (2011); Ch. Skokos, I. Gkolias, and S. Flach, Phys. Rev. Lett. **111**, 064101 (2013).

[7] H. Veksler, Y. Krivolapov, and S. Fishman, Phys. Rev. E **80**, 037201 (2009); A. Pikovsky and S. Fishman, *ibid.* **83**, 025201 (2011); E. Michaely and S. Fishman, *ibid.* **85**, 046218 (2012).

[8] Ch. Skokos and S. Flach, Phys. Rev. E **82**, 016208 (2010).

[9] G. Gligorić, J. D. Bodyfelt, and S. Flach, Europhys. Lett. **96**, 30004 (2011).

[10] S. Fishman, Y. Krivolapov, and A. Soffer, Nonlinearity **25**, R53 (2012), and references therein.

[11] S. Inouye, M. R. Andrews, J. Stenger, H. J. Miesner, D. M. Stamper-Kurn, and W. Ketterle, Nature (London) **392**, 151 (1998).

[12] P. G. Kevrekidis, G. Theocharis, D. J. Frantzeskakis, and B. A. Malomed, Phys. Rev. Lett. **90**, 230401 (2003).

[13] M. Theis, G. Thalhammer, K. Winkler, M. Hellwig, G. Ruff, R. Grimm, and J. H. Denschlag, Phys. Rev. Lett. **93**, 123001 (2004).

[14] C. Chin, R. Grimm, P. Julienne, and E. Tiesinga, Rev. Mod. Phys. **82**, 1225 (2010).

[15] I. L. Garanovicha, S. Longhi, A. A. Sukhorukova, and Y. S. Kivshara, Phys. Rep. **518**, 1 (2012); Y. V. Kartashov, B. A. Malomed, and L. Torner, Rev. Mod. Phys. **83**, 247 (2011); S. Longhi, Opt. Lett. **30**, 2137 (2005); Y. Lahini, F. Pozzi, M. Sorel, R. Morandotti, D. N. Christodoulides, and Y. Silberberg, Phys. Rev. Lett. **101**, 193901 (2008).

[16] A. Szameit and S. Nolte, J. Phys. B **43**, 163001 (2010); S. Longhi, Phys. Rev. A **83**, 034102 (2011); D. Blömer, A. Szameit, F. Dreisow, T. Schreiber, S. Nolte, and A. Tünnermann, Opt. Express **14**, 2151 (2006).

[17] J. Wang and J. B. Gong, Phys. Rev. Lett. **102**, 244102 (2009).

[18] J. B. Gong, L. Morales-Molina, and P. Hänggi, Phys. Rev. Lett. **103**, 133002 (2009).

[19] S. Greschner, G. Sun, D. Poletti, and L. Santos, Phys. Rev. Lett. **113**, 215303 (2014).

[20] F. Meinert, M. J. Mark, K. Lauber, A. J. Daley, and H. C. Nägerl, Phys. Rev. Lett. **116**, 205301 (2016).

[21] G. Casati, B. V. Chirikov, F. M. Izrailev, and J. Ford, in *Stochastic Behavior in Classical and Quantum Hamiltonian Systems*, edited by G. Casati and J. Ford, Lecture Notes in Physics Vol. 93 (Springer, Berlin, 1979).

[22] F. L. Moore, J. C. Robinson, C. F. Bharucha, B. Sundaram, and M. G. Raizen, Phys. Rev. Lett. **75**, 4598 (1995); H. Ammann, R. Gray, I. Shvarchuck, and N. Christensen, *ibid.* **80**, 4111 (1998); M. B. d'Arcy, R. M. Godun, M. K. Oberthaler, D. Cassettari, and G. S. Summy, *ibid.* **87**, 074102 (2001); C. Ryu, M. F. Andersen, A. Vaziri, M. B. d'Arcy, J. M. Grossman, K. Helmerson, and W. D. Phillips, *ibid.* **96**, 160403 (2006); I. Talukdar, R. Shrestha, and G. S. Summy, *ibid.* **105**, 054103 (2010); M. Lopez, J. F. Clement, P. Szriftgiser, J. C. Garreau, and D. Delande, *ibid.* **108**, 095701 (2012); B. Gadway, J. Reeves, L. Krinner, and D. Schneble, *ibid.* **110**, 190401 (2013).

[23] B. Mieck and R. Graham, J. Phys. A: Math. Gen. **38**, L139 (2005).

[24] V. Gelfreich, V. Rom-Kedar, K. Shah, and D. Turaev, Phys. Rev. Lett. **106**, 074101 (2011); K. Shah, Phys. Rev. E **83**, 046215 (2011).

[25] J. Wang, I. Guarneri, G. Casati, and J. B. Gong, Phys. Rev. Lett. **107**, 234104 (2011); H. Wang, J. Wang, I. Guarneri, G. Casati, and J. Gong, Phys. Rev. E **88**, 052919 (2013).

[26] See Appendix for detailed discussions about the properties of the correlation function $Y_n(t)$, for the derivation of Eq. (11), and for the relation between K_g and $g^2 L^2(t)$. There is also numerical confirmation of $\alpha\eta/\beta \approx 2$.